Research Article

Analytic Simulation for Magnetohydrodynamic Unsteady Buongiorno Model Hybrid Nanofluid Flow over Stretching

Muhammad Jawad,[1] Salah Boulaaras [ID],[2] Niaz Ali Shah,[1] Rashid Jan [ID],[1] and Sulima Ahmed Zubair [ID] [2,3]

[1]*Department of Mathematics, University of Swabi, Swabi, 23561 KPK, Pakistan*
[2]*Department of Mathematics, College of Sciences and Arts, Qassim University, Ar Rass, Saudi Arabia*
[3]*Department of Mathematics, College of Sciences, Juba University, Sudan*

Correspondence should be addressed to Sulima Ahmed Zubair; sulimaa2021@gmail.com

In this work, we inspect and analyze a two dimensional, unsteady mixed convectional hybrid nanofluid hydromagnetic flow (Al_2O_3-Cu/H_2O) over a convectional heated an extending/contracting surface with the influence of thermal radiation. Hybrid nanofluid (Al_2O_3-Cu/H_2O) flows with magnetohydrodynamic and heat source or sink. Brownian motion and thermophoresis were incorporated using the Buongiorno model. Hybrid nanofluid with vol. fraction range limited to 1.5% and within the higher temperature range of 50°C to 70°C is considered for thermal conductivity and viscosity analysis. The proposed model is then converted into ODEs through similarity transformation with the help of homotopy analysis. The effect of embedded input factors on the temperature, velocity, and concentration profiles is visually demonstrated and explained. The magnetic field has inverse impact on velocity and temperature profiles. Velocity profile increases for both mixed convection and buoyancy ratio parameters. It has been noticed that the temperature profile increases with thermal radiation. For increasing values of Lewis number, the concentration of hybrid nanoparticles is considerably lowered. Moreover, we observed an increase in the concentration of hybrid nanoparticles through a destructive chemical reaction, whereas a generative chemical reaction has the reverse effect. It has been proved that skin friction is increasing function of ε, M and decreasing function of λ_1, N_r. On the other hand, Nusselt number increased with the increase of R, Q, N_b, N_t while Sherwood number is decreased, with the increase of N_b, N_t, Le.

1. Introduction

It is eminent that many studies have been carried out on two cases of nanoparticles floating in a base fluid known as "Hybrid Nanofluid" the forefront nanofluid. The key importance of the hybrid nanofluid is that by selecting the right mix of nanoparticles, favorable characteristics may be enhanced, and drawbacks can be mitigated owing to their interactive influence. It is reported that these hybrid nanofluids are new and have a number of application acoustics, defense, manufacturing, transportation, medical, microflui-

dics, and naval constructions. Nanofluid flow, in particular, is long familiar for its high heat conveyance when equated to regular fluid. The hybrid nanofluid is applied to raise it even further. Jamshed and Aziz [1] studied the Cattaneo-Christov heat flux impact and discovered that spherical shaped nanoparticles transmit heat at the fastest rate when compared to hexagon, platelet type nanoparticles. The authors in [2] examined squeezing flow in a hybrid base fluid with nanoparticles suspended in it. The hybrid nanofluid stagnation point flow past an extending sheet was investigated by the researchers [3]. The influence on flow

between two riga-plates was investigated by Ahmed et al. [4]. The authors in [5] studied the impact of changing viscosity on a stretched sheet containing hybrid nanoparticles using the Runge–Kutta fourth order technique. The researchers in [6] interrogated the synthesis of hybrid nanofluid while in [7] examined the effects of a hybrid nanofluid of (Al_2O_3-Cu/H_2O) on heat transmission.

There are numerous numerical methods in the literature to inspect the boundary layer flow and heat transport of a hybrid nanofluid. These concepts were further explored by the researchers in their research [9] to conceptualize the main idea. The problem was then expanded to a three-dimensional flow capable to the Newtonian heating consideration by the authors [10]. In both the above studies, they obtained key results about the heat transfer. The difficulty of a hybrid nanofluid consisting of a rotating flow was described by Hayat and Nadeem [11]. Zainal et al. [12] inspected the unsteady stagnation point flow of a hybrid nanofluid past a convectional heated an extending/contracting surface while accounting for velocity slip's influence on heat transfer. Using the Buongiorno model, Daniel et al. [13] investigated an unstable blended convectional electrical magnetohydrodynamic (MHD) flow and heat conveyance generated by nanofluid across a permeable stretched surface. The friction coefficient and wear volume were studied by Xie et al. [14] to determine the tribological properties of hybrid nanoparticles. Devi and Anjali [10] investigated the three-dimensional flow of (Cu-Al_2O_3/water) copper alumina/water hybrid nanofluid using the RK-Fehlberg integration technique.

Thermal radiation's effect on MHD blood flow and heat conveyance in a permeable capillary in extending motion was inspected. It has been examined that at high temperatures, heat transfer and thermal radiation are recognized to have a significant influence on numerous physiological processes, technological, and engineering industry equipment. Solar collector performance, plume dynamics, rocket propulsion, high-dose cancer therapy, fire propagation, material processing, and combustion systems are just a few examples. With the advancement of analytical and computational techniques, thermal convection flows with high radiative flux have received more attention recently. The effect of heat radiation on peristaltic transport of ionic nanoliquids in biomicrofluid channels had analyzed by Prakash et al. [15]. In context from melting heat transfer and thermal radiation, the researcher [16] proposed the dynamics of stagnation point flow of carbon nanotubes. To get series solution, the optimal homotopy technique was used. Muhammad et al. [17] make another notable attempt to address the key aspects of heat radiation and viscous dissipation impacts in a viscous nanofluid. Mixed convectional and slide impacts in viscous nanofluid across an extended sheet were described by Hsiao [18]. The solution was numerically defined using the convective boundary conditions [19]. The reader can further study about heat transfer through nanofluid flow in refs. [20–27]. The relevant study has been seen in [28–31].

The main aim of this research is to see how magnetic fields, thermal radiation, and heat generation/absorption affect unstable hybrid nanofluid hydromagnetic flow (Al_2O_3-Cu/H_2O) across a convectional heated an extend-ing/contracting surface. The thermophoresis and Brownian motion characteristics were included in the Buongiorno model. To minimize the autonomous variables in governance equations resulting from mathematical modelling, a suitable collection of dimensionless variables is employed. By implementing the homotopy approach, an analytical solution has been calculated. Comparison between HAM and ND solve has been shown in Table 1.

2. Mathematical Formulation

Assume the unsteady hybrid nanofluid hydromagnetic flow (Al_2O_3-Cu/H_2O) past a convectional heated an extending/contracting surface in the bearing of the magnetic field, chemical reaction, heat generation/absorption, and thermal radiation. The flow problem plot is depicted in Figure 1, where $u_w(x, t) = bx/(1 - ct)$, the extending/contracting is surface velocity, b indicates a constant that agree to extending ($b > 0$) and contracting($b < 0$) instances, and c denotes the problem of unsteadiness. The velocity of the free stream is notified by $u_e(x, t) = ax/(1 - ct)$, where $a > 0$ is the strength of the stagnation flow. T_1 and T_0 are used to represent the ambient and reference temperature separately. Then, we consider that the bottom of the surface is heated by convectional from a hot fluid at a particular temperature $T_f(x, t) = T_1 - T_0(ax^2/2v)$ $(1 - ct)^{-3/2}$ and coefficient of heat transfer has noted by h_f while the mass transfer coefficient is indicated by h_s. The governing boundary layer equations may be recognized as [12, 13] based on all of the assumptions mentioned.

$$\frac{\partial u}{\partial x} + \frac{\partial u}{\partial y} = 0, \tag{1}$$

$$\frac{\partial u}{\partial t} + u\frac{\partial u}{\partial x} + v\frac{\partial u}{\partial y} = \frac{\partial u_e}{\partial t} + \mu_e\frac{\partial u_e}{\partial x} + \frac{\mu_{hnf}}{\rho_{hnf}}\frac{\partial^2 u}{\partial y^2}$$
$$+ \frac{1}{\rho_{hnf}}\left[(1 - C_\infty)\beta_{hnf}\rho_f(T - T_\infty)\right.$$
$$\left. - (\rho_p - \rho_f)(C - C_\infty)\right]g + \frac{\sigma_{hnf}\beta_0^2}{\rho_{hnf}(1 - ct)}u, \tag{2}$$

$$\frac{\partial T}{\partial t} + u\frac{\partial T}{\partial x} + v\frac{\partial T}{\partial y} = \frac{k_{hnf}}{(\rho c_p)_{hnf}}\frac{\partial^2 T}{\partial y^2} + \frac{1}{(\rho c_p)_{hnf}}\left(\frac{\partial q_r}{\partial y}\right)$$
$$+ \tau\left[D_B\left(\frac{\partial C}{\partial y}\frac{\partial T}{\partial y}\right) + \frac{D_T}{T_\infty}\left(\frac{\partial T}{\partial y}\right)^2\right]$$
$$+ \frac{Q_0}{(\rho c_p)_{hnf}}(T - T_\infty), \tag{3}$$

Applying concept of Rosseland approximation q_r is as follows:

$$q_r = -\frac{4\sigma_1}{3k^*}\frac{\partial T^4}{\partial y}, \tag{4}$$

TABLE 1: Comparison of HAM with ND solve solution $\phi_1 = 0.25$, $\phi_2 = 0.25$, $\varepsilon = 0.3$, $N_r = 1.0$, $\lambda_1 = 0.2$, $Q = 0.5$, $Pr = 6.5$, $M = 0.5$, $R = 0.5$, $Sc = 1.0$, $N_t = 0.2$, $N_b = 0.1$.

η	$f(\eta)$		$f'(\eta)$		$\theta(\eta)$		$\Phi(\eta)$	
	HAM	ND solve	HAM	ND solve	HAM	ND solve	HAM	ND solve
0	0	0	0.02453760	0.02452978	0.487	0.487	0.55	0.55
0.5	0.03469568	0.03468659	0.04076865	0.04056421	0.50874001	0.50873986	0.61285007	0.61284999
1.0	0.06034958	0.06033885	0.20425912	0.20425742	0.51243432	0.51242415	0.55162402	0.55162416
1.5	0.12373158	0.12373098	0.21768635	0.21767085	0.52785902	0.52785899	0.84572417	0.84572406
2.0	0.11524238	0.11519427	0.22753476	0.22753087	0.53762042	0.53761997	0.85465107	0.85465099
2.5	0.28505217	0.28505214	0.10843705	0.10843604	0.54702062	0.54701015	1.04640087	1.04640015
3.0	0.37086918	0.37086908	0.10784304	0.10784291	0.49093352	0.49093295	1.04465601	1.04465592
3.5	0.39292487	0.39292467	0.02030697	0.02030691	0.47529652	0.47529605	1.03547618	1.03547608
4.0	0.40946208	0.40946179	0.02363014	0.02363001	0.48842752	0.48842702	1.03840447	1.03840396
4.5	0.41575308	0.41575305	0.04157226	0.04155423	0.49605602	0.49605595	1.03905327	1.03915306
5.0	0.42407258	0.42407239	0.04216302	0.04216271	0.39754262	0.39754187	1.05743307	1.05743298
5.5	0.44812538	0.44810615	0.04341604	0.04341581	0.35504732	0.35504711	1.05816737	1.05816706
6.0	0.45242414	0.45242409	0.04539012	0.04538997	0.34648862	0.34648795	1.00908797	1.00908706
6.5	0.47365747	0.47365729	0.04683201	0.04683192	0.35742472	0.35703415	0.94253457	0.94253406
7.0	0.49502798	0.49502796	0.04765024	0.04764981	0.37508582	0.37508565	0.92718608	0.92718594
7.5	0.50392098	0.50391896	0.04852079	0.04851972	0.38710902	0.38710875	0.85842701	0.85842689

where the parameters σ_1 and k^* are explained in nomenclature

$$T^4 = 4T_0^4 T - 3T_0^4. \tag{5}$$

Further simplification leads us to the following:

$$(q_r)_y = -\frac{16\sigma_1 T_0^3}{3k^*} T_{yy}. \tag{6}$$

Here, we rewrite Equation (3) as follows:

$$\frac{\partial T}{\partial t} + u\frac{\partial T}{\partial x} + v\frac{\partial T}{\partial y} = \frac{k_{hnf}}{(\rho c_p)_{hnf}}\frac{\partial^2 T}{\partial y^2} + \frac{1}{(\rho c_p)_{hnf}}\left(\frac{\partial q_r}{\partial y}\right) + $$
$$+ \tau\left[D_B\left(\frac{\partial C}{\partial y}\frac{\partial T}{\partial y}\right) + \frac{D_T}{T_\infty}\left(\frac{\partial T}{\partial y}\right)^2\right] \tag{7}$$
$$+ \frac{Q_0}{(\rho c_p)_{hnf}}(T - T_\infty),$$

$$\frac{\partial C}{\partial t} + u\frac{\partial C}{\partial x} + v\frac{\partial C}{\partial y} = D_B\frac{\partial^2 C}{\partial y^2} + \left(\frac{D_T}{T_\infty}\right)T_{yy}, \tag{8}$$

where u denotes the factor of velocity in x-axis, v is the velocity factor in y-axis, μ_{hnf} is the Al_2O_3-Cu/H_2O dynamic viscosity, and D_b and D_t are the Brownian thermophoretic diffusion terms while ρ_{hnf} is the density of Al_2O_3-Cu/H_2O, T is the Al_2O_3-Cu/H_2O temperature, k_{hnf} is the thermal/heat conductivity of Al_2O_3-Cu/H_2O, and $(\rho c_p)_{hnf}$ is the Al_2O_3-Cu/H_2O heat capacity. The boundary conditions, as well as the velocity partial slip, are set to

$$u = u_w(x, t) + H_1 v\frac{\partial u}{\partial y}, v = 0, -k_{hnf}T_y$$
$$= h_f(T_f - T), D_b C_y = h_s(C_f - C) \text{ at } y = 0,$$

$$u \longrightarrow u_e(x, t), T \longrightarrow T_\infty, C \longrightarrow C_\infty \text{ at } y \longrightarrow \infty, \tag{9}$$

where $H_1 = H(1 - ct)^{1/2}$ is the velocity slip term, in which H stands for the starting merit of the velocity slip term. Table 2 lists the thermophysical characteristics of copper (Cu), as well as aluminium oxide (Al_2O_3) and water (H_2O) nanoparticles. The thermophysical characteristics of hybrid nanofluid are shown in Table 3. The solid volume fraction of nanoparticles is described as ϕ, where ρ_f denotes the density, ρ_s is the density of the hybrid nanoparticle, c_p is the constant pressure of heat capacity, k_f represents the thermal conductivity of H_2O, and k_s is the thermal conductivity of the hybrid nanoparticle.

The follower similarity transformations are provided in order to represent the governed Equations (1), (2), (7), and (8) concerning the BCs (9) in a much easy way [12].

$$\psi = \left(\frac{av}{1 - ct}\right)^{1/2} xf(\eta), \theta(\eta) = \frac{T - T_\infty}{T_f - T_\infty},$$

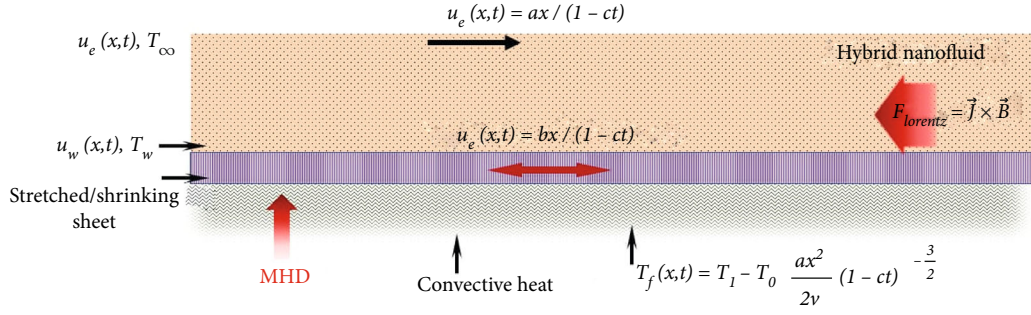$$\Phi(\eta) = \frac{C - C_\infty}{C_f - C_\infty}\eta = \left(\frac{a}{v(1 - ct)}\right)^{1/2} y, \tag{10}$$

FIGURE 1: Schematic diagram of the 2D flow past a stretching/shrinking sheet.

TABLE 2: Cu thermophysical properties along with Al_2O_3 and H_2O [12].

Thermophysical properties	Cu	Al_2O_3	H_2O
k(W/mK)	400	40	0.613
ρ(kg/m^3)	8933	3970	9971
c_p(J/kgK)	385	765	4179
$\beta \times 10^5$(1/K)	1.67	0.85	21

where ψ is the stream function that can be specified as $u = \partial\psi/\partial y$ and $v = -\partial\psi/\partial x$ and η is the similarity variable. Thus, we attain

$$u = \frac{ax}{1-ct}f'(\eta), v = -\left(\frac{av}{1-ct}\right)^{1/2}f(\eta). \quad (11)$$

Equations (2), (7), and (8) are converted into the following set of nonlinear similarity ODEs by using the similarity variables (10) and (11) in light of the aforementioned relationships.

$$\frac{\mu_{hnf}/\mu_f}{\rho_{hnf}/\rho_f}f''' + 2ff'' - f'^2 + 1 - \varepsilon\left(f' - \frac{1}{2}\eta f'' - 1\right)$$
$$- \lambda\frac{\beta_{hnf}}{\beta}\left[\theta - \frac{N_r}{\beta_{hnf}/\beta}\phi\right] + \frac{\sigma_{hnf}/\sigma_f}{\rho_{hnf}/\rho_f}Mf' = 0, \quad (12)$$

$$\frac{1}{Pr}\frac{1}{(\rho c_p)_{hnf}/(\rho c_p)_f}\left(\frac{k_{hnf}}{k_f} + \frac{4}{3}R\right)\theta'' + f\theta' - 2f'\theta$$
$$+ \frac{\varepsilon}{2}\left(\eta\theta' + 3\theta\right) + \left[N_b\theta'\Phi' + N_t\theta'^2\right] + \frac{Q(\rho c_p)_f}{(\rho c_p)_{hnf}}\theta = 0, \quad (13)$$

$$\Phi'' + Scf\Phi' - Sc\frac{\varepsilon}{2}\left(\eta\Phi' + 3\Phi\right) + \frac{N_t}{N_b}\theta'' = 0. \quad (14)$$

Now the starting and final constraints (9) are also changed into the following:

$$f(0) = 0, f'(0) = \lambda + \gamma f''(0),$$

$$-\frac{k_{hnf}}{k_f}\theta'(0) = Bi[1 - \theta(0)],$$

$$\Phi'(0) = -N_d(1 - \Phi(0)),$$

$$f'(\eta) \longrightarrow 1, \theta(\eta) \longrightarrow 0, \Phi(\eta) \longrightarrow 0, \text{ while } \eta \longrightarrow \infty, \quad (15)$$

where $\varepsilon, M, R, Pr, N_r, Bi, Re_x, \lambda, Q, \lambda_1, Sc, N_t,$ and N_b are unsteadiness parameter, magnetic parameter, thermal radiation parameter, Prandtl number, buoyancy ratio parameter, Biot number, local Reynolds number in x-axis, ratio of velocity parameter, heat source/sink parameter, mixed convection parameter, Lewis number, thermophoretic parameter, and Brownian motion parameter.

$$\varepsilon = \frac{c}{a}, M = \frac{\sigma\beta_0^2}{\rho_f a}, \gamma = H(av)^{1/2},$$

$$Bi = \frac{h_f}{k_f}\sqrt{\frac{v(1-ct)}{a}},$$

$$Re_x = \frac{u_e x}{v}, R = \frac{4\sigma^* T_\infty^3}{3k^* k_f},$$

$$Q = \frac{Q_0(1-ct)^2}{ax}, Pr = \frac{v}{\alpha},$$

$$N_r = \frac{(\rho_p - \rho_f)\Delta C}{\rho_f\beta(1 - C_\infty)\Delta T},$$

$$\lambda = \frac{b}{a}, \lambda_1 = \frac{Gr}{(Re_x)^2},$$

$$Sc = \frac{v}{D_B}, N_t = \frac{\tau D_T(T_s - T_0)}{v_f T_0},$$

$$N_b = \frac{\tau D_B(C_w - C_\infty)}{v_f}. \quad (16)$$

TABLE 3: Applied models for thermophysical properties of the hybrid nanofluid [12].

Property	Hybrid nanofluid
Viscosity	$\mu_{hnf} = 1/\left(1 - \phi_{hnf}\right)^{2.5}$
Density	$\rho_{hnf} = \left(1 - \phi_{hnf}\right)\rho_f + \phi_1\rho_{s1} + \phi_2\rho_{s2}$
Thermal capacity	$\left(\rho c_p\right)_{hnf} = \left(1 - \phi_{hnf}\right)\left(\rho c_p\right)_f + \phi_1\left(\rho c_p\right)_{s1} + \phi_2\left(\rho c_p\right)_{s2}$
Thermal conductivity	$k_{hnf}/k_f = \left[\left(\left(\phi_1 k_{s1} + \phi_2 k_{s2}/\phi_{hnf}\right) + 2k_f + 2(\phi_1 k_{s1} + \phi_2 k_{s2}) - 2\phi_{hnf}k_f/\left(\phi_1 k_{s1} + \phi_2 k_{s2}/\phi_{hnf}\right) + 2k_f - 2(\phi_1 k_{s1} + \phi_2 k_{s2}) - \phi_{hnf}k_f\right]$
Electrical conductivity where	$\sigma_{hnf}/\sigma_{nf} = \left[\sigma_{s2} + \sigma_{nf} - 2\phi_2(\sigma_{nf} - \sigma_{s2})/\sigma_{s2} + 2\sigma_{nf} + \phi_2(\sigma_{nf} - \sigma_{s2})\right]$ $\sigma_{nf}/\sigma_f = \left[\sigma_{s1} + 2\sigma_f - 2\phi_1(\sigma_f - \sigma_{s1})/\sigma_{s1} + 2\sigma_f + \phi_1(\sigma_f - \sigma_{s1})\right]$
Thermal expansion	$(\rho\beta)_{hnf} = \left\{(1 - \phi_2)\left(1 - \phi_1\right) + (1 - \phi_2)\phi_1\left((\rho\beta)_{s1}/(\rho\beta)_f\right)\right\} + \phi_2\left((\rho\beta)_{s2}/(\rho\beta)_f\right)$

2.1. *Physical Quantities of Interest.* For above model local Nusselt number (Nu_x), the skin friction coefficient (c_f) and Sherwood number are clear as follows:

$$c_f = \frac{\tau_w}{\rho_f u_e^2}, Nu_x = \frac{xq_w}{k_f(T_f - T_\infty)}, Sh_x = \frac{xq_m}{D_B(C_f - C_\infty)},$$

(17)

where

$$\tau_w = \mu_{hnf}\left(\frac{\partial u}{\partial y}\right)_{y=0},$$

$$q_w = -k_{hnf}\left(\frac{\partial T}{\partial y} - q_r\right)\bigg|_{y=0},$$

$$q_m = -D_b(C_y)_{y=0}.$$

(18)

In dimensional form, we have from above as

$$[\mathrm{Re}_x]^{1/2}C_f = \frac{\mu_{hnf}}{\mu_f}f''(0),$$

$$[\mathrm{Re}_x]^{-1/2}Nu_x = -\frac{k_{hnf}}{k_f}\left(1 + \frac{4}{3}R\right)\theta'(0),$$

$$[\mathrm{Re}_x]^{-1/2}Sh = -\phi'(0).$$

(19)

2.2. *Idea of HAM for the Model.* Here, we used HAM to solve Equations (12)–(14) using boundary conditions (15). The Mathematica software is utilized for this, and the proposed model can be solved using HAM in the following manner:

$$L_{\widehat{f}}\left(\widehat{f}\right) = \widehat{f}''' - \widehat{f}', L_{\widehat{\theta}}\left(\widehat{\theta}\right) = \widehat{\theta}'' - \widehat{\theta}, L_{\widehat{\Phi}}\left(\widehat{\Phi}\right) = \widehat{\Phi}'' - \widehat{\Phi},$$

(20)

where operators are specified as $L_{\widehat{f}}$ and $L_{\widehat{\theta}}$; moreover, we have

$$L_{\widehat{f}}(\gamma_1 + \gamma_2 e^{-\eta} + \gamma_3 e^{\eta}) = 0, L_{\widehat{\theta}}(\gamma_4 e^{-\eta} + \gamma_5 e^{\eta})$$
$$= 0, L_{\widehat{\phi}}(\gamma_6 e^{-\eta} + \gamma_7 e^{\eta}) = 0.$$

(21)

We also define the operators, such that

$$N_{\widehat{f}}\left[\widehat{f}(\eta;\zeta), \widehat{\theta}(\eta;\zeta), \widehat{\Phi}(\eta;\zeta)\right]$$
$$= \frac{\mu_{hnf}/\mu_f}{\rho_{hnf}/\rho_f}\widehat{f}_{\eta\eta} + 2\widehat{f}\widehat{f}_{\eta\eta} - \widehat{f}_\eta^2 + 1 - \varepsilon\left(\widehat{f}_\eta - \frac{1}{2}\eta\widehat{f}_{\eta\eta} - 1\right)$$
$$- \lambda\frac{\beta_{hnf}}{\beta}\left[\widehat{\theta} - \frac{N_r}{\beta_{hnf}/\beta}\widehat{\Phi}\right] + \frac{\sigma_{hnf}/\sigma_f}{\rho_{hnf}/\rho_f}M\widehat{f}_\eta,$$

$$N_{\widehat{\theta}}\left[\widehat{f}(\eta;\zeta), \widehat{\theta}(\eta;\zeta)\right] = \frac{1}{\mathrm{Pr}}\frac{1}{(\rho c_p)_{hnf}/(\rho c_p)_f}\left(\frac{k_{hnf}}{k_f} + \frac{4}{3}R\right)\widehat{\theta}_{\eta\eta}$$
$$+ \widehat{f}\widehat{\theta}_\eta - 2\widehat{f}_\eta\widehat{\theta} + \frac{\varepsilon}{2}\left(\eta\widehat{\theta}_\eta + 3\widehat{\theta}\right)$$
$$+ \frac{\tau_{hnf}}{(\tau/v)_f}\left[N_b\widehat{\theta}'\widehat{\Phi}' + N_t\widehat{\theta}'^2\right]$$
$$+ \frac{Q(\rho c_p)_f}{(\rho c_p)_{hnf}}\widehat{\theta},$$

$$N_{\widehat{\Phi}}\left[\widehat{\Phi}(\eta;\zeta), \widehat{f}(\eta;\zeta), \widehat{\theta}(\eta;\zeta)\right]$$
$$= \widehat{\Phi}_{\eta\eta} + Sc\widehat{f}\widehat{\Phi}_\eta - Sc\widehat{f}_\eta\widehat{\Phi} - Sc\frac{\varepsilon}{2}\left(\eta\widehat{\Phi}_\eta + 3\widehat{\Phi}\right) + \frac{N_t}{N_b}\widehat{\theta}''.$$

(22)

For Equations (12)–(14), the 0th-order system is shown as follows:

$$(1 - \zeta)L_{\widehat{f}}\left[\widehat{f}(\eta;\zeta) - \widehat{f}_0(\eta)\right] = p\hbar_{\widehat{f}}N_{\widehat{f}}\left[\widehat{f}(\eta;\zeta)\right],$$

$$(1 - \zeta)L_{\widehat{\theta}}\left[\widehat{\theta}(\eta;\zeta) - \widehat{\theta}_0(\eta)\right] = p\hbar_{\widehat{\theta}}N_{\widehat{\theta}}\left[\widehat{\theta}(\eta;\zeta), \widehat{f}(\eta;\zeta)\right],$$

$$(1 - \zeta)L_{\widehat{\Phi}}\left[\widehat{\Phi}(\eta;\zeta) - \widehat{\Phi}_0(\eta)\right] = p\hbar_{\widehat{\Phi}}N_{\widehat{\Phi}}\left[\widehat{\Phi}(\eta;\zeta), \widehat{f}(\eta;\zeta), \widehat{\theta}(\eta;\zeta)\right],$$

(23)

with the BCs are

$$\widehat{f}(\eta;\zeta)\bigg|_{\eta=0} = 0, \frac{\partial\widehat{f}(\eta;\zeta)}{\partial\eta}\bigg|_{\eta=0} = \lambda + \gamma\frac{\partial^2\widehat{f}(\eta;\zeta)}{\partial\eta^2}\bigg|_{\eta=0}, f(0) = 0,$$

$$\frac{k_{nf}}{k_f}\frac{\partial\widehat{\theta}(\eta;\zeta)}{\partial\eta}\bigg|_{\eta=0} = -Bi\left(1 - \widehat{\theta}(0)\right), \frac{\partial\widehat{\Phi}(\eta;\zeta)}{\partial\eta}\bigg|_{\eta=0}$$
$$= -N_d\left(1 - \widehat{\Phi}(0)\right)$$

$$\frac{\partial\widehat{f}(\eta;\zeta)}{\partial\eta}\bigg|_{\eta=\infty} \longrightarrow 1, \widehat{\theta}(\eta;\zeta)\bigg|_{\eta=\infty} \longrightarrow 0, \widehat{\Phi}(\eta;\zeta)\bigg|_{\eta=\infty} \longrightarrow 0.$$

(24)

While the embedding constraint is $\zeta \in [0, 1]$, to regulate for the solution convergence $\hbar_{\widehat{f}}, \hbar_{\widehat{\theta}}$, and $\hbar_{\widehat{\Phi}}$ are used. At specific values $\zeta = 0$ and $\zeta = 1$, the following is obtained:

$$\widehat{f}(\eta;1) = \widehat{f}(\eta), \widehat{\theta}(\eta;1) = \widehat{\theta}(\eta), \widehat{\Phi}(\eta;1) = \widehat{\Phi}(\eta).$$

(25)

Expand the $\widehat{f}(\eta;\zeta)$, $\widehat{\theta}(\eta;\zeta)$, and $\widehat{\Phi}(\eta;\zeta)$ through Taylor's series for $\zeta = 0$

$$\widehat{f}(\eta;\zeta) = \widehat{f}_0(\eta) + \sum_{n=1}^{\infty} \widehat{f}_n(\eta)\zeta^n,$$

$$\widehat{\theta}(\eta;\zeta) = \widehat{\theta}_0(\eta) + \sum_{n=1}^{\infty} \widehat{\theta}_n(\eta)\zeta^n,$$

$$\widehat{\Phi}(\eta;\zeta) = \widehat{\Phi}_0(\eta) + \sum_{n=1}^{\infty} \widehat{\Phi}_n(\eta)\zeta^n,$$

$$\widehat{f}_n(\eta) = \frac{1}{n!}\frac{\partial\widehat{f}(\eta;\zeta)}{\partial\eta}\bigg|_{p=0},$$

$$\widehat{\theta}_n(\eta) = \frac{1}{n!}\frac{\partial\widehat{\theta}(\eta;\zeta)}{\partial\eta}\bigg|_{p=0},$$

$$\widehat{\Phi}_n(\eta) = \frac{1}{n!}\frac{\partial\widehat{\Phi}(\eta;\zeta)}{\partial\eta}\bigg|_{p=0}. \tag{26}$$

While BCs are

$$\widehat{f}(0) = 0, \widehat{f}'(0) = \lambda + \gamma\widehat{f}''(0),$$

$$\frac{k_{hnf}}{k_f}\widehat{\theta}'(0) = -Bi\left(1 - \widehat{\theta}(0)\right), \widehat{\Phi}'(0) = -N_d\left(1 - \widehat{\Phi}(0)\right),$$

$$\widehat{f}'(\eta) \longrightarrow 0, \widehat{\theta}(\eta) \longrightarrow 0, \widehat{\Phi}(\eta) \longrightarrow 0 \eta \longrightarrow \infty.$$

$$\mathfrak{R}_n^{\widehat{f}}(\eta) = \frac{\mu_{hnf}/\mu_f}{\rho_{hnf}/\rho_f}\widehat{f}'''_{n-1} + 2\sum_{j=0}^{w-1}\widehat{f}_{w-1-j}\widehat{f}''_j - \widehat{f}'^2_{n-1}$$

$$+ 1 - \varepsilon\left(\widehat{f}'_{n-1} - \frac{1}{2}\eta\widehat{f}_{n-1} - 1\right) + \frac{\sigma_{hnf}/\sigma_f}{\rho_{hnf}/\rho_f}M\widehat{f}'_{n-1}$$

$$- \lambda\left[\widehat{\theta}_{n-1} - N_r\widehat{\Phi}_{n-1}\right],$$

$$\mathfrak{R}_n^{\widehat{\theta}}(\eta) = \frac{1}{\Pr}\frac{1}{(\rho c_p)_{hnf}/(\rho c_p)_f}\left(\frac{k_{hnf}}{k_f} + \frac{4}{3}R\right)\left(\widehat{\theta}''_{n-1}\right)$$

$$+ \sum_{j=0}^{w-1}\widehat{\theta}'_{w-1-j}\widehat{f}_j - 2\sum_{j=0}^{w-1}\widehat{\theta}_{w-1-j}\widehat{f}'_j +$$

$$\frac{\varepsilon}{2}\left(\eta\widehat{\theta}'_{n-1} + 3\widehat{\theta}_{n-1}\right) + \frac{\tau_{hnf}}{(\tau/\upsilon)_f}\left[N_b\sum_{j=0}^{w-1}\widehat{\theta}'_{w-1-j}\widehat{\Phi}'_j + N_t\widehat{\theta}'^2_{n-1}\right]$$

$$+ \frac{Q(\rho c_p)_f}{(\rho c_p)_{hnf}}\widehat{\theta}_{n-1},$$

$$\mathfrak{R}_n^{\widehat{\Phi}}(\eta) = \widehat{\Phi}''_{n-1} + Sc\sum_{j=0}^{w-1}\widehat{f}_{w-1-j}\widehat{\Phi}'_j - Sc\sum_{j=0}^{w-1}\widehat{f}'_{w-1-j}\widehat{\Phi}_j$$

$$+ \frac{N_t}{N_b}\widehat{\theta}''_{n-1} + Sc\frac{\varepsilon}{2}\left(\eta\widehat{\Phi}'_{n-1} + 3\widehat{\Phi}_{n-1}\right). \tag{27}$$

While

$$\chi_n = \begin{cases} 0, & \text{if } n \leq 1, \\ 1, & \text{if if } n > 1. \end{cases} \tag{28}$$

3. Outcomes with Discussion

In the following discussion section, the outcomes of various parametric quantity on velocity, concentration profiles, and temperature are shown graphically and discussed. These parameters are unsteadiness parameter, buoyancy ratio parameter, magnetic parameter, thermal radiation parameter, Lewis number, mixed convection parameter, Prandtl number and thermophorotic parameter, and Brownian motion parameter. The geometry of the problem is shown in Figure 1. It can be seen that when the magnetic parameter M assigns maximum values, the velocity distribution retains its declining tendency as shown in Figure 2. There is a periodic oscillation velocity with diminishing amplitude while the magnetic force produces a resistive nature force known as the Lorentz force which controls the flow of fluid particles. As a result, to demonstrate the value of reducing the velocity of moving particles, the effect of the unsteadiness parameter on ε the nanofluid velocity profile has seen in Figure 3. Because of the acceleration situation, $(\varepsilon > 0)$ brings down rate of fluid flow and a narrower momentum boundary barrier thickness; the behavior occurs. The velocity profile reduces for the higher acceleration.

Figure 4 illustrates the influence of the buoyancy ratio parameter on velocity drawings and also increasing levels of N_r; there is a noticeable increase in velocity. This increase in velocity drawings is more noticeable in stable condition than in the unsteadness situation. Figure 5 shows the effect of λ_1 on $f'(\eta)$. From Figure 5, it can be expected that $f'(\eta)$ has greater values of λ_1. Physically, this is because of the larger values of buoyancy force. The impact of heat generation/absorption on the temperature is plotted in Figure 6. The temperature of the fluid and the thickness of the thermal boundary level are both increased when a heat source $(Q > 0)$ is used. The heat sink $(Q < 0)$, on the other hand, lowers the fluid's temperature and thins the thermal boundary level thickness.
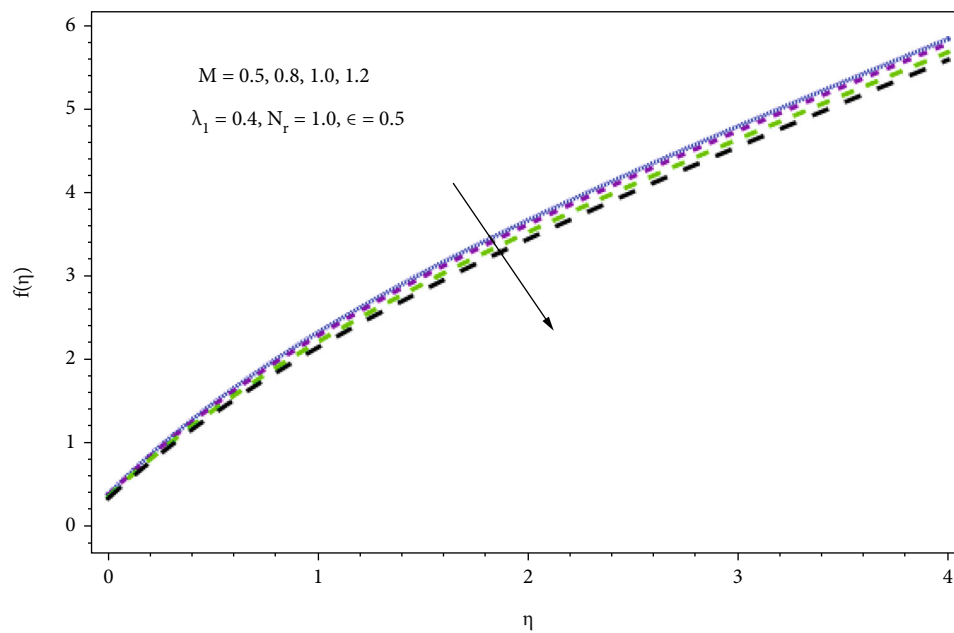
FIGURE 2: Illustration of the effect of M on $f'(\eta)$.
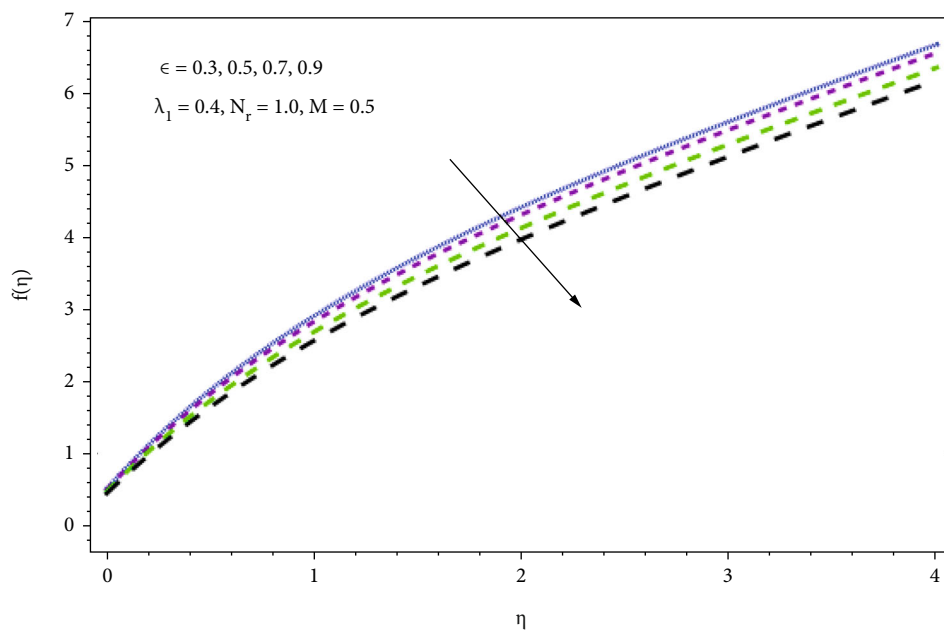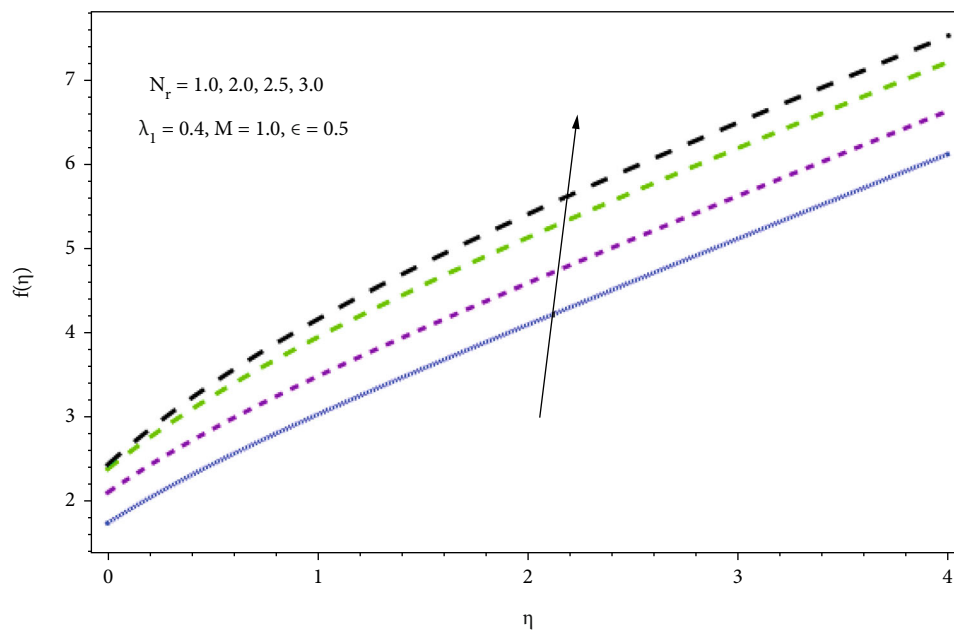

FIGURE 3: Representation of the effect of ε on $f'(\eta)$.

$N_r = 1.0, 2.0, 2.5, 3.0$

$\lambda_1 = 0.4, M = 1.0, \epsilon = 0.5$

FIGURE 4: Illustration of the effect of N_r on $f'(\eta)$.

$\lambda_1 = 0.2, 0.6, 1.1, 1.2$

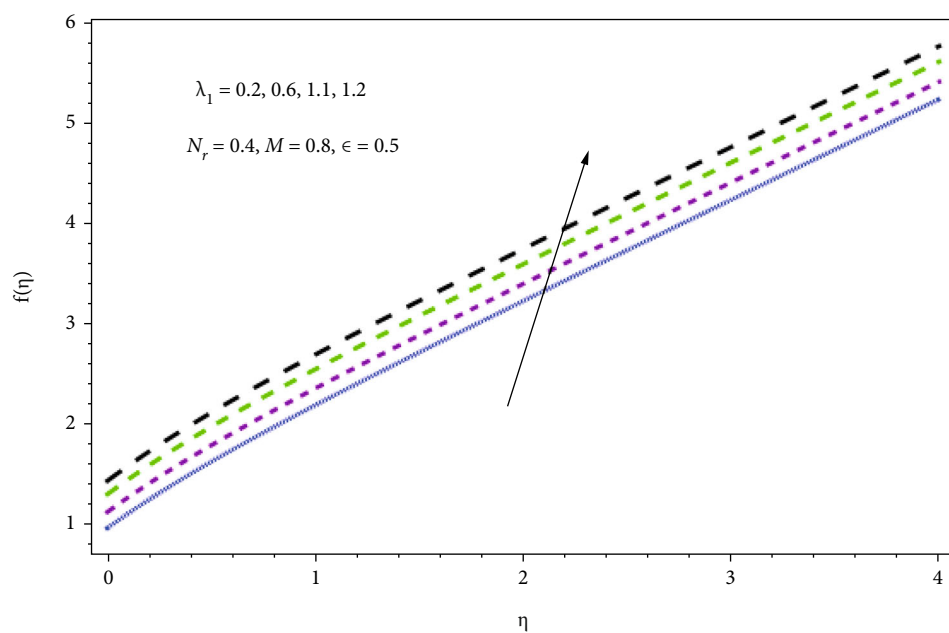$N_r = 0.4, M = 0.8, \epsilon = 0.5$

FIGURE 5: Illustration of the effect of λ_1 on $f'(\eta)$.
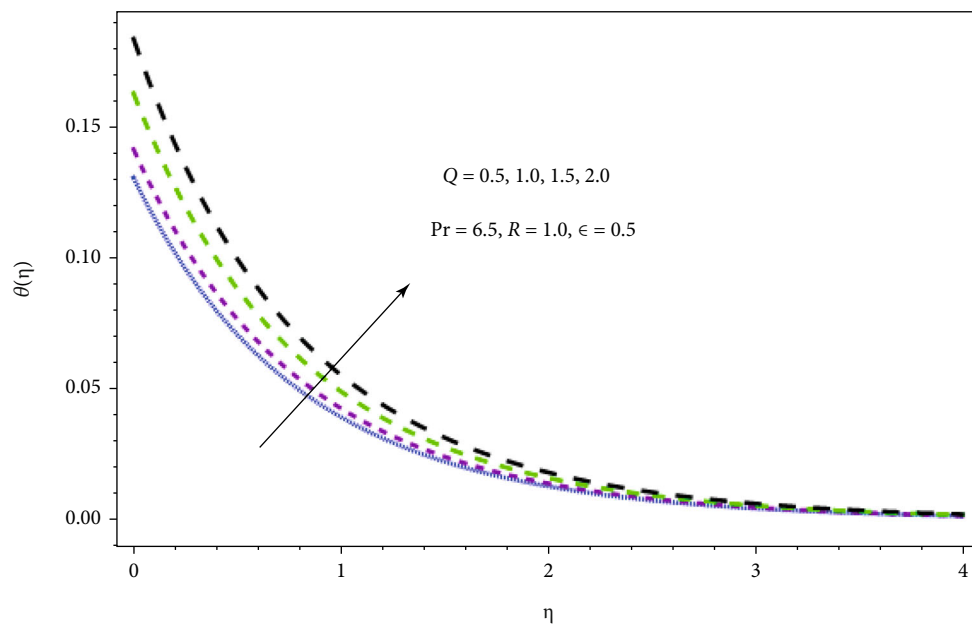
FIGURE 6: Illustration of the effect of Q on $\theta(\eta)$.
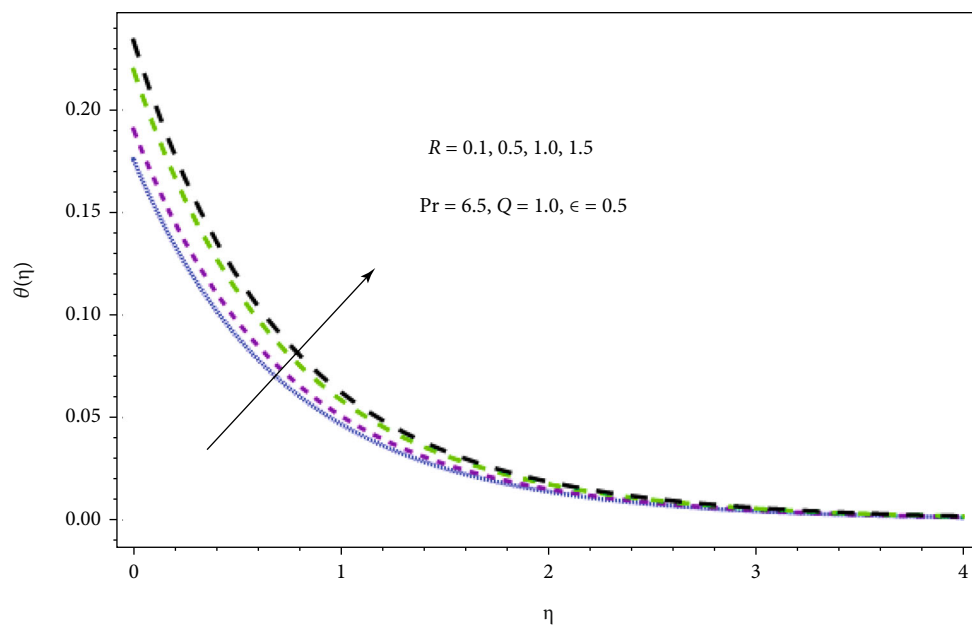

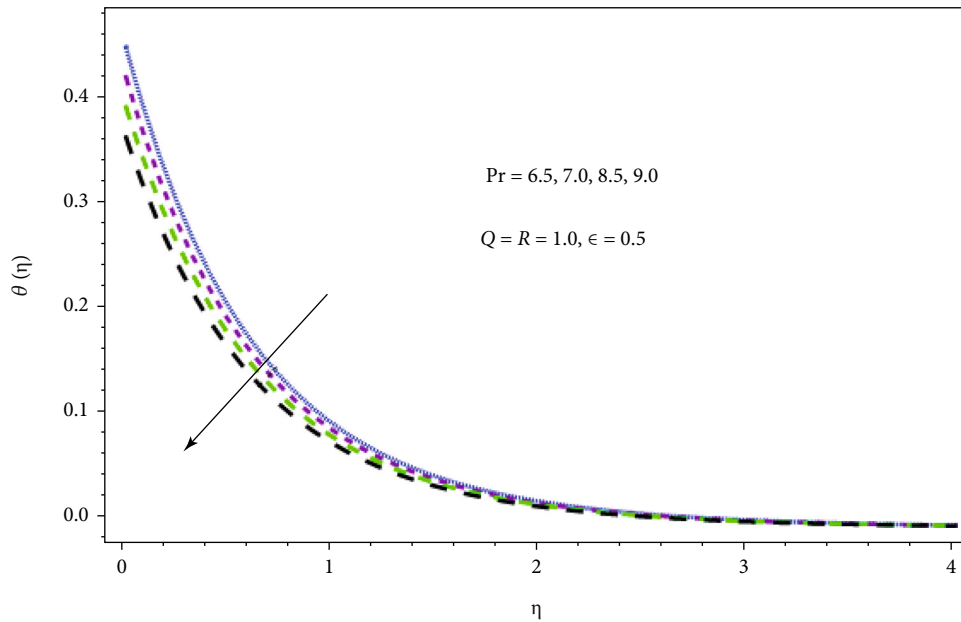FIGURE 7: Representation of the effect of R on $\theta(\eta)$.

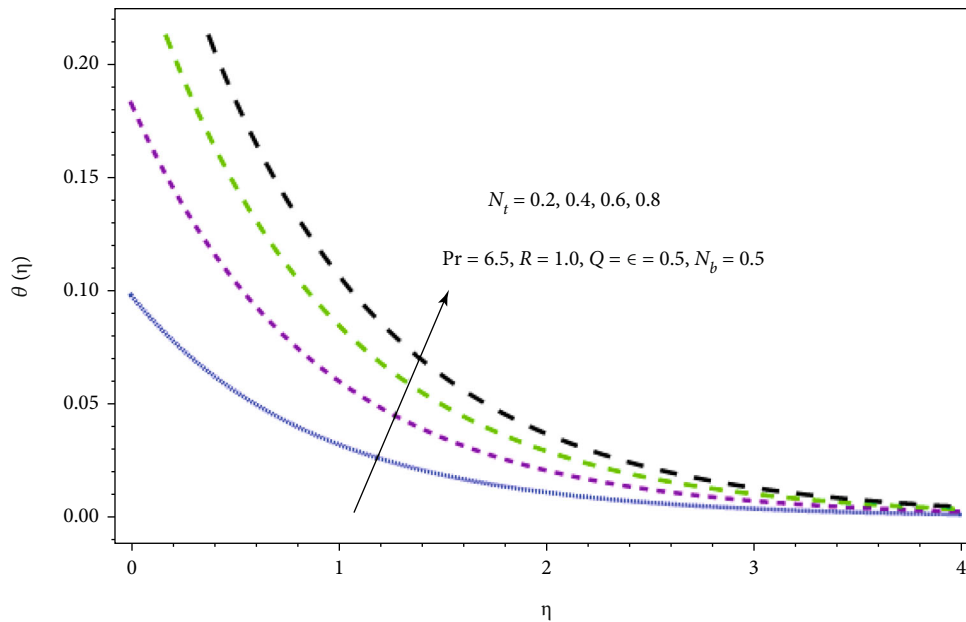FIGURE 8: Graphical view to show the effect of Pr on $\theta(\eta)$.

FIGURE 9: Illustration of the effect of N_t on $\theta(\eta)$.

To denote $(Q = 0)$, the lack of heat generation or absorption, the increase in thermal radiation raises the temperature but lowers the concentration profiles, as seen in Figure 7. This is because an increase in thermal radiation gives to a greater extent heat to the hybrid nanofluid, resulting in a rise in temperature and the thickness of the thermal boundary layer. Physically, radiative aspect creates the Brownian motion of minute ingredients faster than normal; thus, random migrated particles strike with one another, and the caused frictional energy transforms it to thermal energy.

The effect from the Prandtl number along the temperature profile has seen in Figure 8. By increasing the Prandtl number, the fluid's thermal conductivity decreases. This fact is due to inverse relation of Pr with thermal diffusivity, and it is well-known fact that the fluid with higher values of Pr has weaker thermal diffusion so that the temperature declines. Figures 9 and 10 demonstrate the consequence of the thermophoresis parametric quantity (N_t) along the thermal profile. When the thermophoresis parametric quantity is increased which enhance the behavior of the system,
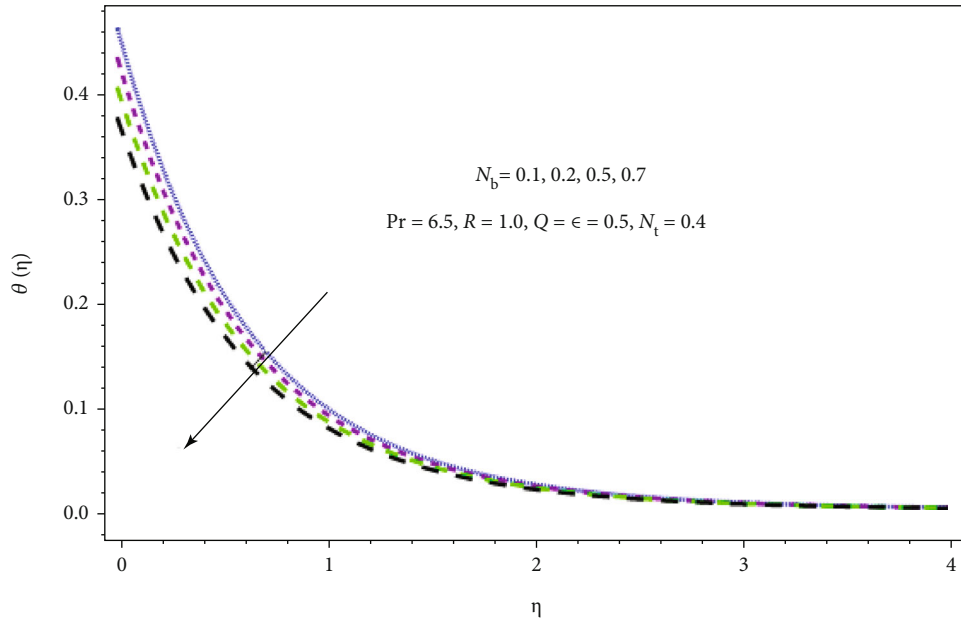
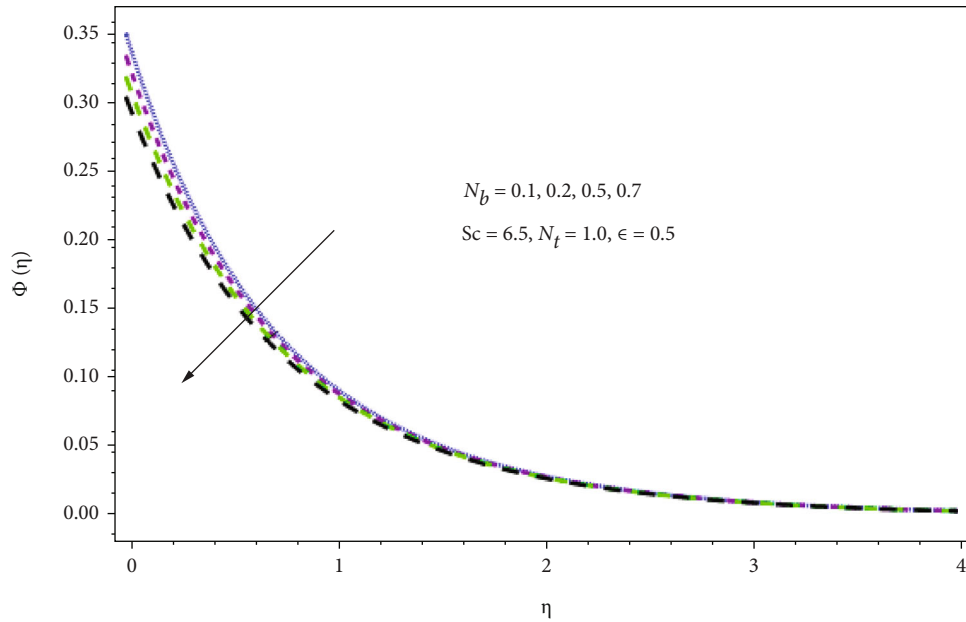FIGURE 10: Graphical view of the effect of N_b on $\theta(\eta)$.

FIGURE 11: Representation of the effect of N_b on $\Phi(\eta)$.

thermophoresis effect is associated with movement of nanoparticles from a hot wall to a cold wall, and since it is generated by temperature gradients, it creates a fast flow away from the moving plate; thus, more fluid is heated away from the surface, and this leads to an increase in the temperature within the thermal boundary layer. Figure 10 demonstrates the consequence of the Brownian diffusion parameter (N_b) on the thermal profile. Physically, the imperfect nature of the Brownian motion parametric quantity enables heating the physical setup. This heating causes nanoparticles to be transferred from the cooler stretched sheet area to the quiescent fluid zone. Because the particles migrate from a high up to a low concentration part, an increase in the Brownian motion parameter N_b and $\Phi(\eta)$ leads decrease in the fluid concentration gradient, as seen in Figure 11.

The Brownian motion is the movement of fluid particles from higher to lower concentration so increases in the thermophoresis parameter (N_t) produce a huge rise in the concentration dispersion of the fluid flow $\Phi(\eta)$, which meet to zero at the boundary level, as shown in Figure 12. A minor

$N_t = 0.2, 0.4, 0.6, 0.8$
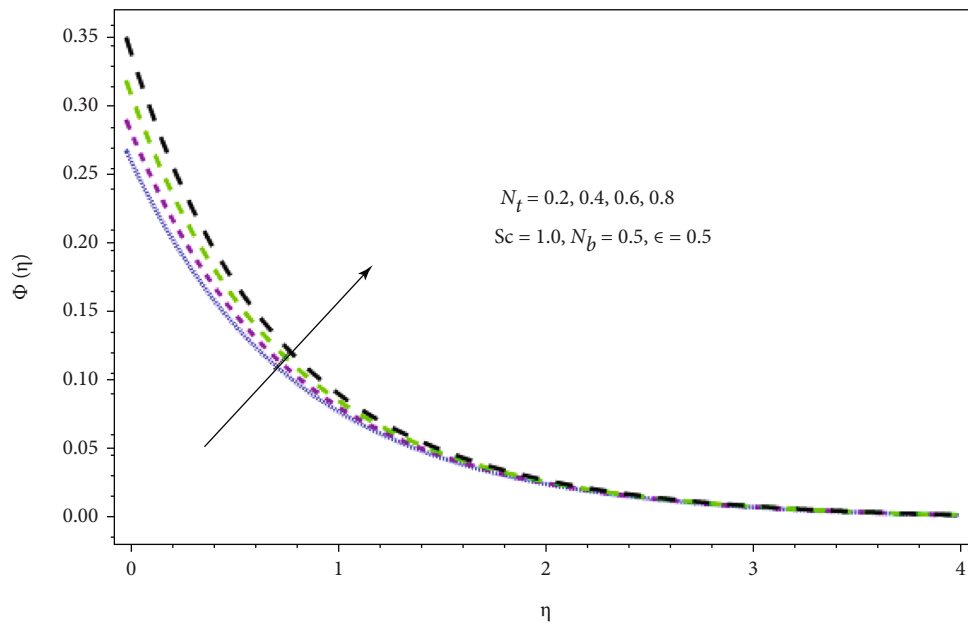
$Sc = 1.0, N_b = 0.5, \epsilon = 0.5$

FIGURE 12: Illustration of the effect of N_t on $\Phi(\eta)$.

$Sc = 0.5, 1.0, 1.5, 1.8$

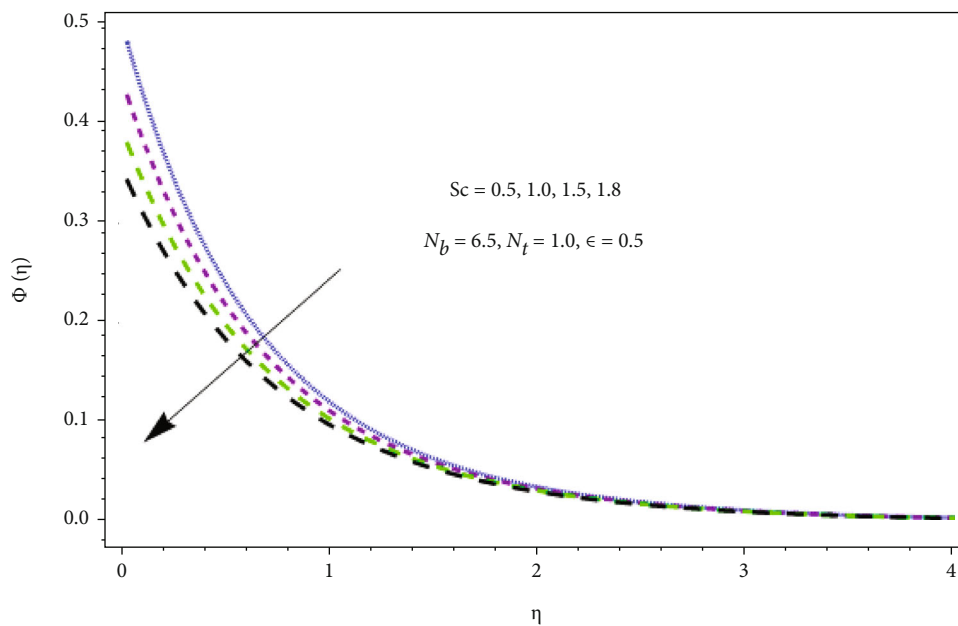$N_b = 6.5, N_t = 1.0, \epsilon = 0.5$

FIGURE 13: Representation of the effect of Sc on $\Phi(\eta)$.

TABLE 4: Representation of the influence of different physical factors on skin friction $[\mathrm{Re}_x]^{1/2}C_f = (\mu_{hnf}/\mu_f)f''(0)$.

λ_1	N_r	M	ε	$\left(\mu_{hnf}/\mu_f\right)f''(0)$
0.3	0.3	0.5	0.3	1.6735237
0.5				1.4321803
1.0				1.2307539
	0. 3			2.2316739
	0.5			2.1317693
	1.0			2.1038033
		0.5		1.3156063
		1.0		1.4367109
		1.5		1.4837333
			0.3	2.1396853
			0.5	2.1946379
			0.7	2.2453103

TABLE 5: Illustration of the influence of different physical factors over Nusselt number $[\mathrm{Re}_x]^{-1/2}Nu_x = -(k_{hnf}/k_f)(1+(4/3)R)\theta'(0)$.

R	Q	Pr	N_t	N_b	ε	$-\left(k_{hnf}/k_f\right)(1+4/3R)\theta'(0)$
0.8	-0.5	7.5	0.7	0.5	0.3	1.8363904
1.0						1.7214318
1.2						1.3274134
	-0.5					1.3435906
	-1.0					1.1643153
	-1.5					1.0366173
		7.5				1.3453139
		8.5				1.6437058
		9.5				1.8467893
			0.2			1.2327811
			0.4			1.1364383
			0.6			1.0953647
				0.3		1.4735333
				0.7		1.3794531
				0.9		1.2393407
					0.3	1.6157203
					0.5	1.7240367
					0.7	1.8090526

TABLE 6: Illustration of the influence of different physical factors over Sherwood number $\mathrm{Re}\,s^{-1/2}Sh_x = -\phi'(0)$..

N_t	N_b	Le	$-\phi'(0)$
0.2	0.3	2.0	2.1493731
0.4			2.1730691
0.6			2.2393414
	0.3		2.3518701
	0.7		2.4504103
	0.9		2.4993798
		2.0	2.5623087
		3.3	2.6573919
		4.0	2.6935286

4. Discussion on Tabulated Results

Table 4 shows that C_f is increased when the values of ε, M are increased. The C_f is decreased, when the values of λ_1, N_r are increased. Table 5 shows that Nu_x is increased when the values of R, Q, N_b, N_t are increased. The Nu_x is decreased, when the values of Pr are increased. Table 6 shows that Sh is decreased, when the values of N_b, N_t, Le are increased. Table 1 shows the very excellent agreement of the HAM and ND solve solution by computer-based package Mathematica 11.1.0.

5. Conclusions

In this research work, the uniform mixed convectional with the combined consequences of thermal radiation and heat generation/absorption along the magnetohydrodynamic (MHD) flow of hybrid nanofluid via a convectional heated the stretching/shrinking surface is studied. Brownian motion and thermophoresis were incorporated using the Buongiorno model. We came at the following key conclusions based on our findings with various factors in this study:

(i) Increasing the combined convection and buoyancy ratio parameters improved nanofluid flow properties

(ii) It is well established that an increase in the unsteadiness and magnetic parameters result in a decrease in the velocity profile

(iii) Consequently, a rise in the thermophorotic parameter, radiation parameter, or Brownian motion parameter means an increase in the temperature profile

(iv) It is noticed that the increase of the Prandtl number decreases the temperature profile

(v) Increases in the values of the thermophoretic parameter and Brownian motion parameter have an inverse influence on the concentration profile

(vi) The $\Phi(\eta)$ displays lessening tendency for rising values of Le

change in the thermophoresis parameter causes the fluid particles to move quickly, releasing surplus heat energy and causing a huge rise in the concentration dispersion. As a result, with an increase in the value of (N_t), Figure 12 indicates a considerable rise in the concentration dispersion. Figure 13 also shows the influence of the Schmidt number on the concentration dispersion. It is noticed that for larger values of Sc, the fluid concentration decreases. This fact is quite similar with that of Prandtl number impact on temperature. Actually, Sc has inverse relation with mass diffusivity; therefore, larger values of Sc correspond thinner concentration boundary layer.

(vii) Skin friction is augmented when the values of ε, M are improved. When the values of λ_1, N_r is enlarged, C_f is reduced

(viii) Nusselt number is improved when the values R, Q, N_b, N_t are increased. The Nu_x is reduced, when the values of Pr are augmented

(ix) Sherwood number is declined, when the values of N_b, N_t, Le are enlarged

Nomenclature

u and v: Components of velocity along x- and y-axes (m/s)
u_w: Stretching/shrinking velocity (m/s)
T_1:   Ambient temperature (K)
h_f: Heat transfer coefficient
μ_{hnf}:   (kgm^{-1}s^{-1}) Viscosity of hybrid nanofluid
Re$_x$:   Reynolds number
θ: Dimensionless temperature
ρ_s: The density of the nanoparticle (kgm^{-3})
k_s: Nanoparticle thermal conductivity (Wm^{-1}K^{-1})
ψ: Stream function
M: Magnetic parameter
H_1:   Velocity slip factor
λ: Ratio of velocity parameter and heat
Nu_x: Local Nusselt number
f':   Dimensionless velocity
v: Kinematic viscosity (m^{2}s^{-1})
q_m: Wall mass flux
q_r: Rosseland approximation
ϕ: Nanoparticle solid volume fraction
k^*:   Coefficient of mean absorption
C_f: Plate concentration
C_∞:   Concentration of ambient
h_s: Mass transfer coefficient
N_b: Brownian motion parameter
x, y: Cartesian coordinate axis
u_e: Strength of the stagnation flow
T_0:   Reference temperature (K)
ρ_{hnf}:   Hybrid nanofluid density (kgm^{-3})
$(\rho c_p)_{hnf}$:   Hybrid nanofluid volumetric heat capacity (m^{2}s^{-2}K^{-1})
H: Initial value of the velocity slip factor
c_p: Constant pressure of heat capacity
ρ_f: Base fluid density (kgm^{-3})
k_f: Base fluid thermal conductivity (Wm^{-1}K^{-1})
ε: Unsteadiness parameter
Φ: Dimensionless concentration
Pr: Prandtl number
Q: Source/sink parameter
c_f: Skin friction coefficient
T: Temperature of fluid (K)
μ_f: Dynamic viscosity (kgm^{-1}s^{-1})
τ_w: Wall shear stress
q_w: Transportation of heat
σ^*:   Stefan-Boltzmann constant
k_1:   Porosity parameter

R: Thermal radiation parameter
C_w: Wall concentration
Bi: Biot number
N_t: Thermophoretic parameter.

Data Availability

No data were used to support this study.

Conflicts of Interest

The authors declare that they have no conflicts of interest.

References

[1] W. Jamshed and A. Aziz, "Cattaneo–Christov based study of TiO$_2$–CuO/EG Casson hybrid nanofluid flow over a stretching surface with entropy generation," *Applied Nanoscience*, vol. 8, no. 4, pp. 685–698, 2018.

[2] S. S. Ghadikolaei, M. Gholinia, M. E. Hoseini, and D. D. Ganji, "Natural convection MHD flow due to MoS$_2$–Ag nanoparticles suspended in C$_2$H$_6$O$_2$–H$_2$O hybrid base fluid with thermal radiation," *Journal of the Taiwan Institute of Chemical Engineers*, vol. 97, pp. 12–23, 2019.

[3] S. S. Ghadikolaei, M. Yassari, H. Sadeghi, K. Hosseinzadeh, and D. D. Ganji, "Investigation on thermophysical properties of Tio$_2$-Cu/H$_2$O hybrid nanofluid transport dependent on shape factor in MHD stagnation point flow," *Powder Technology*, vol. 322, pp. 428–438, 2017.

[4] N. Ahmed, F. Saba, U. Khan et al., "Spherical shaped (Ag–Fe$_3$O$_4$/H$_2$O) hybrid nanofluid flow squeezed between two riga plates with nonlinear thermal radiation and chemical reaction effects," *Energies*, vol. 12, no. 1, p. 76, 2019.

[5] S. Manjunatha, B. A. Kuttan, S. Jayanthi, A. Chamkha, and B. J. Gireesha, "Heat transfer enhancement in the boundary layer flow of hybrid nanofluids due to variable viscosity and natural convection," *Heliyon*, vol. 5, no. 4, article e01469, 2019.

[6] S. Suresh, K. Venkitaraj, P. Selvakumar, and M. Chandrasekar, "Synthesis of Al$_2$O$_3$-Cu/water hybrid nanofluids using two step method and its thermo physical properties," *Colloids and Surfaces A: Physicochemical and Engineering Aspects*, vol. 388, no. 1-3, pp. 41–48, 2011.

[7] S. Suresh, K. Venkitaraj, P. Selvakumar, and M. Chandrasekar, "Effect of Al$_2$O$_3$-Cu/water hybrid nanofluid in heat transfer," *Experimental Thermal and Fluid Science*, vol. 38, pp. 54–60, 2012.

[8] S. Suresh, K. P. Venkitaraj, M. S. Hameed, and J. Sarangan, "Turbulent heat transfer and pressure drop characteristics of dilute water based Al$_2$O$_3$Cu hybrid nanofluids," *Journal of Nanoscience and Nanotechnology*, vol. 14, pp. 2563–2572, 2014.

[9] S. P. A. Devi and S. S. U. Devi, "Numerical investigation of hydromagnetic hybrid Cu – Al$_2$O$_3$/water nanofluid flow over a permeable stretching sheet with suction," *International Journalof Nonlinear Sciences and Numerical Simulation*, vol. 17, no. 5, pp. 249–257, 2016.

[10] S. S. U. Devi and S. P. A. Devi, "Numerical investigation of three-dimensional hybrid Cu–Al$_2$O$_3$/water nanofluid flow over a stretching sheet with effecting Lorentz force subject to Newtonian heating," *Canadian Journal of Physics*, vol. 94, no. 5, pp. 490–496, 2016.

[11] T. Hayat and S. Nadeem, "Heat transfer enhancement with Ag-CuO/water hybrid nanofluid," *Results in Physics*, vol. 7, pp. 2317–2324, 2017.

[12] N. A. Zainal, R. Nazar, K. Naganthran, and I. Pop, "Unsteady stagnation point flow of hybrid nanofluid past a convectively heated stretching/shrinking sheet with velocity slip," *Mathematics*, vol. 8, no. 10, p. 1649, 2020.

[13] Y. S. Daniel, Z. A. Aziz, Z. Ismail, and F. Salah, "Double stratification effects on unsteady electrical MHD mixed convection flow of nanofluid with viscous dissipation and Joule heating," *Journal of Applied Research and Technology*, vol. 15, no. 5, pp. 464–476, 2017.

[14] H. Xie, B. Jiang, B. Liu, Q. Wang, J. Xu, and F. Pan, "An investigation on the tribological performances of the SiO_2/ MoS_2 hybrid nanofluids for magnesium alloy-steel contacts," *Nanoscale Research Letters*, vol. 11, no. 1, pp. 329–336, 2016.

[15] J. Prakash, A. Sharma, and D. Tripathi, "Thermal radiation effects on electroosmosis modulated peristaltic transport of ionic nanoliquids in biomicrofluidics channel," *Journal of Molecular Liquids*, vol. 249, pp. 843–855, 2018.

[16] T. Hayat, K. Muhammad, M. Farooq, and A. Alsaedi, "Melting heat transfer in stagnation point flow of carbon nanotubes towards variable thickness surface," *AIP Advances*, vol. 6, no. 1, article 015214, 2016.

[17] K. Muhammad, T. Hayat, S. A. Shehzad, and A. Alsaedi, "Viscous dissipation and Joule heating effects in MHD 3D flow with heat and mass fluxes," *Results in Physics*, vol. 8, pp. 365–371, 2018.

[18] K. L. Hsiao, "Stagnation electrical MHD nanofluid mixed convection with slip boundary on a stretching sheet," *Applied Thermal Engineering*, vol. 98, no. 5, pp. 850–861, 2016.

[19] B. Mahanthesh, B. J. Gireesha, and R. S. R. Gorla, "Nonlinear radiative heat transfer in MHD three-dimensional fow of water based nanofuidover a non-linearly stretching sheet with convective boundary condition," *Journal of the Nigerian Mathematical Society*, vol. 35, pp. 78–98, 2016.

[20] S. Murtaza, M. Iftekhar, F. Ali, and I. Khan, "Exact analysis of non-linear electro-osmotic flow of generalized Maxwell nanofluid: applications in concrete based nano-materials," *IEEE Access*, vol. 8, pp. 96738–96747, 2020.

[21] N. Mezouar and S. M. Boulaaras, "Global existence and decay of solutions of a singular nonlocal viscoelastic system with damping terms," *Topological Methods in Nonlinear Analysis*, vol. 56, no. 1, pp. 1–312, 2020.

[22] J. Ahmad, F. Ali, S. Murtaza, and I. Khan, "Caputo time fractional model based on generalized Fourier's and Fick's laws for Jeffrey nanofluid: applications in automobiles," *Mathematical Problems in Engineering*, vol. 2021, Article ID 4611656, 12 pages, 2021.

[23] S. M. Boulaaras, A. Choucha, A. Zara, M. Abdalla, and B. B. Cheri, "Global existence and decay estimates of energy of solutions for a new class of -Laplacian heat equations with logarithmic nonlinearity," *Journal of Function Spaces*, vol. 2021, Article ID 5558818, 11 pages, 2021.

[24] F. Ali, S. Murtaza, N. A. Sheikhand, and I. Khan, "Heat transfer analysis of generalized Jeffery nanofluid in a rotating frame: Atangana-Balaenu and Caputo-Fabrizio fractional models," *Chaos, Solitons & Fractals*, vol. 129, pp. 1–15, 2019.

[25] S. Boulaaras and M. Haiour, "The finite element approximation of evolutionary Hamilton-Jacobi-Bellman equations with nonlinear source terms," *Indagationes Mathematicae*, vol. 24, no. 1, pp. 161–173, 2013.

[26] S. Toualbia, A. Zaraï, and S. Boulaaras, "Decay estimate and non-extinction of solutions of p-Laplacian nonlocal heat equations," *AIMS Mathematics*, vol. 5, no. 3, pp. 1663–1679, 2020.

[27] S. Boulaaras, "Some new properties of asynchronous algorithms of theta scheme combined with finite elements methods for an evolutionary implicit 2-sided obstacle problem," *Mathematical Methods in the Applied Sciences*, vol. 40, no. 18, pp. 7231–7239, 2017.

[28] N. Acharya, R. Bag, and P. K. Kundu, "On the impact of nonlinear thermal radiation on magnetized hybrid condensed nanofluid flow over a permeable texture," *Applied Nanoscience*, vol. 10, no. 5, pp. 1679–1691, 2020.

[29] N. Acharya, "On the flow patterns and thermal behaviour of hybrid nanofluid flow inside a microchannel in presence of radiative solar energy," *Journal of Thermal Analysis and Calorimetry*, vol. 141, no. 4, pp. 1425–1442, 2020.

[30] N. Acharya and F. Mabood, "On the hydrothermal features of radiative Fe_3O_4–graphene hybrid nanofluid flow over a slippery bended surface with heat source/sink," *Journal of Thermal Analysis and Calorimetry*, vol. 143, no. 2, pp. 1273–1289, 2021.

[31] N. Acharya, "Spectral quasi linearization simulation on the radiative nanofluid spraying over a permeable inclined spinning disk considering the existence of heat source/sink," *Applied Mathematics and Computation*, vol. 411, article 126547, 2021.